Last Name __Girosco__ **Given Name** ___Pio__ **ID Number** ___20170130__

Question n. 1

Which is the typical range of frequencies at which MEMS gyroscopes (as studied during the course) operate, and why? In case of mode-split operation, which is the typical split value, and why?

Which would possible advantages and drawbacks be in operating a mode-split MEMS gyroscope around higher frequencies, e.g., around 100 kHz?

MEMS gyroscopes for consumer applications are usually operated with the drive and the sense frequencies around or above 20 kHz. There are three major reasons for this choice:

I. *<u>rejection of accelerations and vibrations</u>: accelerations occur generally at low frequencies (and are thus not modulated around the drive frequency), and ideally represent common-mode signals in typical tuning fork gyroscope configurations.*
However, effects of external accelerations may be orders of magnitude larger – in terms of absolute resulting displacement – than those of Coriolis forces. In presence of process nonuniformities (e.g. small gap differences between the differential sensing electrodes) part of their contribution may turn into a differential signal. As the displacement caused by accelerations goes with the inverse of the squared frequency:

$$y_S = \frac{\vec{a}}{\omega_s^2}$$

it is better not to lower too much the operating frequency of gyroscopes;

II. *<u>rejection of acoustic disturbances</u>: gyroscopes are often operated in harsh acoustic environment, e.g. close to loudspeakers or microphones inside smartphones. To avoid disturbances from acoustic signals (and following electronic signal processing), it is better to operate gyroscopes off the audio bandwidth, i.e. at frequencies around or larger than 20 kHz;*

III. *<u>thermomechanical noise</u>: for a given maximum area occupation (i.e. a given mass), for a given drive displacement, and for a given packaging condition (i.e. a given damping), thermomechanical noise goes with the inverse of the sense frequency:*

$$NERD = \frac{180}{\pi}\frac{1}{x_{D,0}\, m_S\, \omega_S}\sqrt{k_B T\, b_S}$$

and it is thus preferable to operate gyroscopes at relatively large frequencies.

In case of mode-split operation, the mode split value sets the trade-off between sensitivity and bandwidth, according (i) to the expression of the scale factor between displacement induced by the Coriolis force and the angular rate

$$\frac{y_s}{\Omega} = \frac{x_d}{\Delta\omega_{MS}}$$

and, (ii), to the fact that the bandwidth is limited to maximum $2\pi\Delta\omega_{MS}$, usually $\frac{1}{3}$ to $\frac{1}{2}$ of this value depending on how the electronic filter is tailored to prevent signal distortion at rate frequencies approaching the mismatch, as shown by the figure. For typical requirements of gyroscope bandwidth in the order of few 100 Hz, a typical mode-split value will be from 500 Hz to about 1 kHz. Larger values would give no further benefits for the desired bandwidth, and would on the contrary reduce the sensitivity and in turn worsen noise performance.

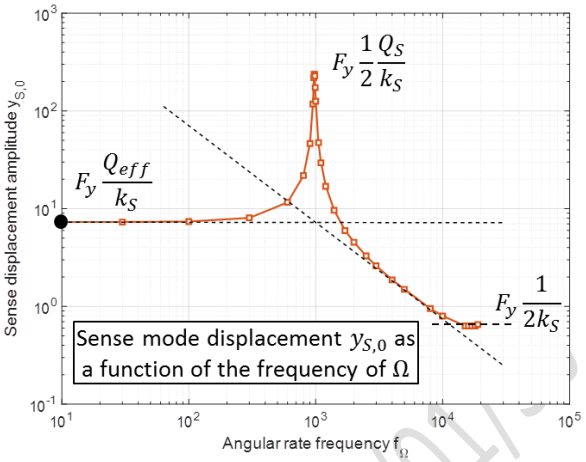

The second part of the question may give rise to a wide discussion…, and it is thus convenient to look at the fundamental parameters of a gyroscope to properly focus the attention. Within these parameters, we should certainly include (i) overall noise density, (ii) offset and, again, (iii) rejection to disturbances.

I. *concerning the overall noise density, we have the thermomechanical contribution that benefits from an increase in the operating frequency, as already discussed above.*
On the other side, we know that all noise contributions (including electronic noise) can be referred as input angular rate through the sensitivity $x_{D,0}/\Delta\omega_{MS}$, and thus through the inverse of the drive displacement amplitude $x_{D,0}$.
For a given area occupation (i.e. a given mass), we note that increasing the drive frequency by large values implies an increase in the drive stiffness.
For a given maximum applicable drive voltage, this results in a lower displacement $x_{D,0}$, thus in a lower sensitivity, and in turn into a worsening of overall noise density performance;

II. *concerning offset, we remind here that the major offset source of gyroscope is given by coupling of quadrature errors with demodulation phase errors. As the input-referred quadrature value is linear with the operating frequency:*

$$B_q = \frac{\alpha}{2}\omega_D$$

we observe that operating at larger frequencies increases the quadrature error. This is the major drawback that usually limits the operating frequencies to the values mentioned above (i.e. around 20 kHz);

III. *finally, concerning rejection to disturbances given by accelerations and vibrations, we observe that a larger operating frequency makes the gyroscope more immune to such issues.*
This is, in conclusions, the sole reason why gyroscopes for industrial, military and automotive applications are generally designed with a larger operating frequency (e.g. 50 kHz).
For such applications, going to even larger frequencies (e.g. 100 kHz) would be beneficial, provided that suitable means for quadrature error compensation (either in the electronics, or through electromechanical effects) are provided to bypass the quadrature increase indicated above.

NOTE: this is just one example of a "good" answer. Other interesting considerations can be added to the discussion, as some of you did during the exam.

Last Name __Girosco__ **Given Name** ___Pio__ **ID Number** ___20170130__

Question n. 2

A polysilicon Z-axis MEMS magnetometer based on the Lorentz force is depicted in Fig. (a). It is formed by two symmetric halves, connected by a tuning fork. In each half, a set of sustaining springs holds a frame in which differential parallel plate capacitors are embedded. It is operated off-resonance, with a split of 300 Hz.

On top of the magnetometer polysilicon springs, an insulating SiO_2 layer is deposited. On top of this insulating layer, a metal loop is deposited. In operation, the driving current flows through the metal loop as in Fig. (b).

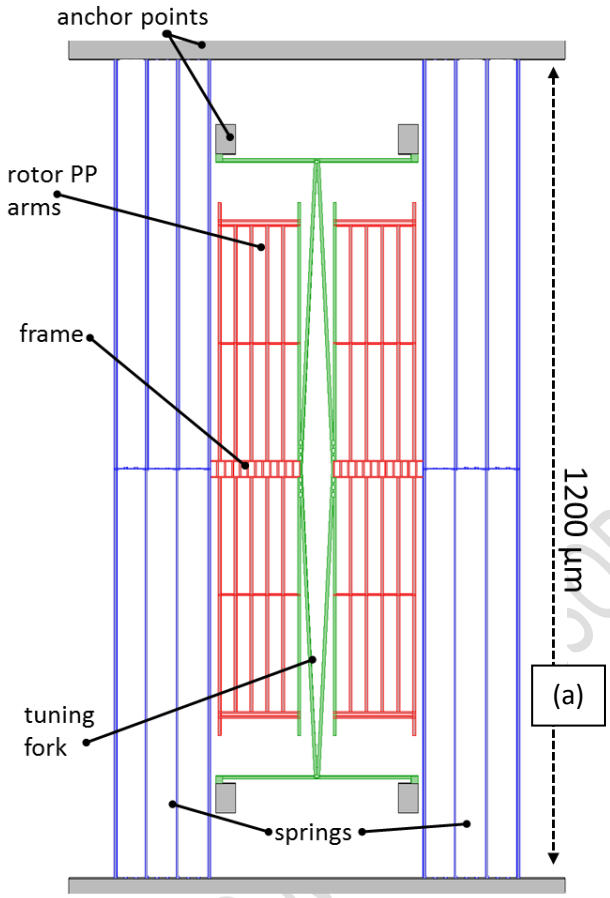

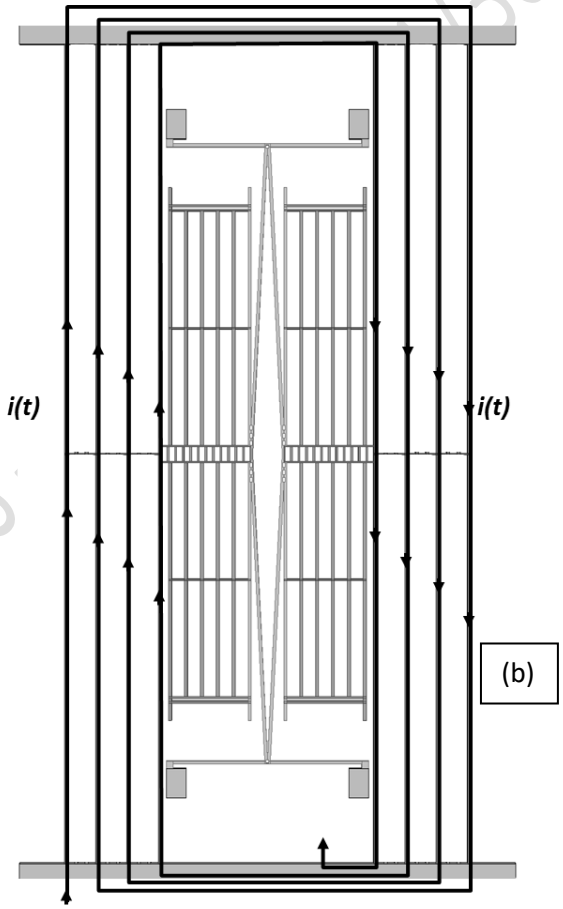

For the parameters given in the Table:

(i) derive the expression of the device sensitivity, expressed in terms of differential capacitance variation per unit magnetic field change [F/T];

(ii) calculate the overall noise density (in terms of input-referred magnetic field). Why is the performance of this magnetometer so good?

(iii) considering that the width of the metal layer can be made (and spaced) as small as 500 nm, suggest a solution to further boost the sensitivity – and quantify the effects on device sensitivity and noise.

Parameter	Symbol	Value
Permittivity of vacuum	ε_o	$8.8 \cdot 10^{-12}$ F/m
Boltzmann constant	k_B	$1.4 \cdot 10^{-23}$ J/K
Process height	H	10 µm
Effective mass (half structure)	m	$1.2 \cdot 10^{-9}$ kg
Resonance frequency	f_0	45 kHz
Parallel plate gap	g	1.8 µm
N of springs (half structure)	N_S	10
Total area of PP cells (single-ended)	A_{PP}	12000 $(\mu m)^2$
Spring length (see figure)	L_S	1200 µm
Spring width	w_S	5 µm
Quality factor	Q	4000
Driving current amplitude	i	50 μA_{rms}
Rotor bias voltage	V_{DC}	15 V
Amplifier voltage noise density	S_{Vn}	$(5\ nV/\sqrt{Hz})^2$
Amplifier feedback capacitance	C_F	400 fF
Amplifier parasitic capacitance	C_P	3 pF

(i)

We are dealing with an off-resonance Lorentz-Force MEMS magnetometer. The interesting concept introduced in this design is represented by the fact that on top of each spring the deposited metal path is separated from the polysilicon by a thin insulating oxide layer. With this architecture, 10 current loops are defined.

The device mechanical sensitivity can be conveniently derived starting from the following sub-transfer functions:

$$\frac{\Delta \mathrm{C}}{\Delta \mathrm{B}} = \frac{\Delta \mathrm{F}}{\Delta \mathrm{B}} \cdot \frac{\Delta \mathrm{x}}{\Delta \mathrm{F}} \cdot \frac{\Delta \mathrm{C}}{\Delta \mathrm{x}}$$

Expanding each term, we can derive the correct formula of the mechanical sensitivity.

$$\frac{\Delta F}{\Delta B} = i_{peak} L_s N_{loop}$$

Where $i_{peak} = \sqrt{2} \cdot i_{rms}$.

$$\frac{\Delta x}{\Delta F} = \frac{\mathrm{Q_{eff}}}{2k_{\frac{1}{2}}}$$

Where $k_{\frac{1}{2}} = \omega_0^2 \cdot m = 96 \frac{N}{m}$ *is the half-structure stiffness and* $Q_{eff} = \frac{f_0}{2 \cdot \Delta f} = 75$ *is effective quality factor for the considered mismatch. The factor 2 at the denominator accounts for the distributed nature of the Lorentz force across the springs.*

$$\frac{\Delta C}{\Delta x} = \frac{2C_0}{g}$$

Where $C_0 = \frac{\epsilon_0 A_{PP}}{g} = 59fF$ *is the whole-structure single-ended rest capacitance, and the factor 2 accounts for the differential readout*.

Finally, the mechanical sensitivity formula can be thus expressed as:

$$\frac{\Delta C}{\Delta B} = i_{peak} L_s N_{loop} \cdot \frac{Q_{eff}}{2k_{\frac{1}{2}}} \cdot \frac{2C_0}{g} = 21 \frac{fF}{T}$$

(ii)

The expression of the noise equivalent magnetic field density (or NEMD) is the following:

$$NEMD = \sqrt{S_{Bn}} = \frac{4}{i_{peak} L N_{loop}} \cdot \sqrt{k_B T b} = 125 \frac{nT}{\sqrt{Hz}}$$

Where $b = \frac{k_{tot}}{\omega_0 Q} = 169 \frac{nN}{\frac{m}{s}}$.

For what concerns the electronics contribution to the overall noise, it is useful to compute first of all the sensitivity expressed in [V/T], considering a TCA readout scheme:

$$S = \frac{\Delta C}{\Delta x} \cdot \frac{V_{DC}}{C_F} = 0.8 \frac{V}{T}$$

The noise voltage density at the differential TCA output is amplified through the ratio of the parasitic capacitance over the feedback capacitance, and it can be thus referred to the input in terms of magnetic field density as follows:

$$\sqrt{S_{B,eln}} = \frac{\sqrt{2S_{vn}} \cdot \left(1 + \frac{C_p}{C_F}\right)}{S} = 65 \frac{nT}{\sqrt{Hz}}$$

Thus, the overall noise density turns out to be:

$$\sqrt{S_{B,TOT}} = \sqrt{S_{B,n} + S_{B,eln}} = 140 \frac{nT}{\sqrt{Hz}}$$

The performance of the magnetometer is so good because we are biasing the moving mass at 15 V, a quite high value: this is compatible with a multi-loop architecture only if the metal and the polysilicon are decoupled through an insulating layer, as in the proposed geometry. Otherwise, the voltage difference between the rotor and the stator would be limited approximately to the mean value of the circuit biasing voltage, i.e. about few V.

(iii)

Again thanks to the presence of the oxide, we can fit five $500nm$ *wide metal paths on every single* $5\mu m$ *thick spring (for sake of simplicity, the oxide layer is not represented in figure):*

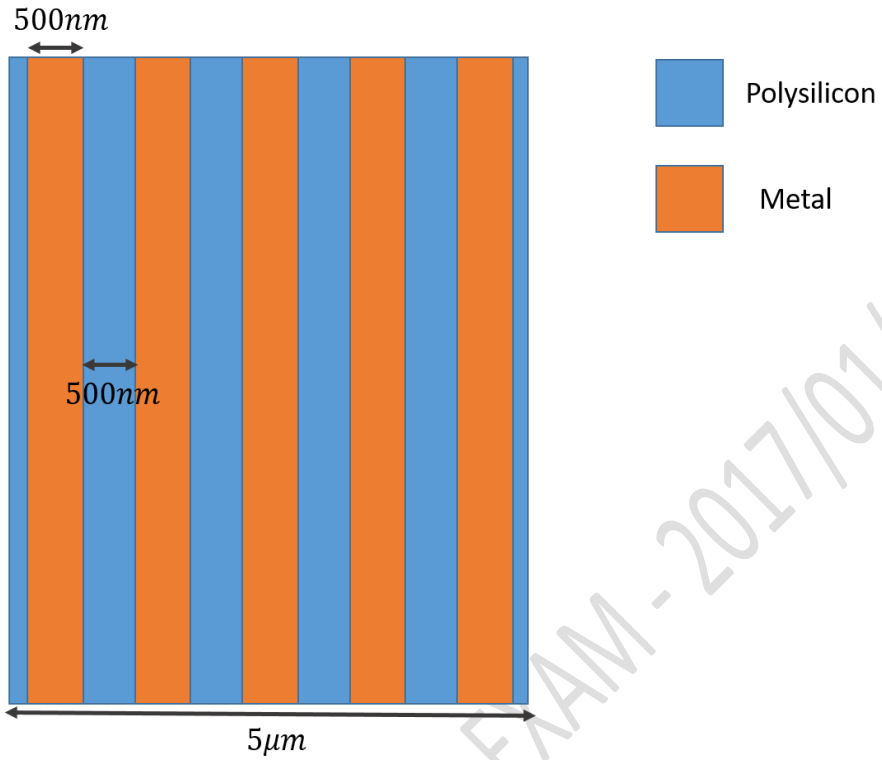

Adopting a similar solution, we can define up to 50 loops within the same occupied area, with overall beneficial effects on both sensitivity and noise:

$$S_{new} = 5 \cdot S = 4\frac{V}{T}$$

$$\sqrt{S_{B,TOT,new}} = \frac{\sqrt{S_{B,TOT}}}{5} = 25\frac{nT}{\sqrt{Hz}}$$

Last Name __Girosco__ **Given Name** ___Pio__ **ID Number** ___20170130__

Question n. 3

The Photon Transfer Curve (PTC) of a 4T CMOS image sensor is first captured at a fixed integration time t_{int1} = 1 ms, while varying the illumination intensity. The result is represented in the graph below as a continuous curve. The sensor pixels, whose size is $(3\ um)^2$, are backside illuminated.

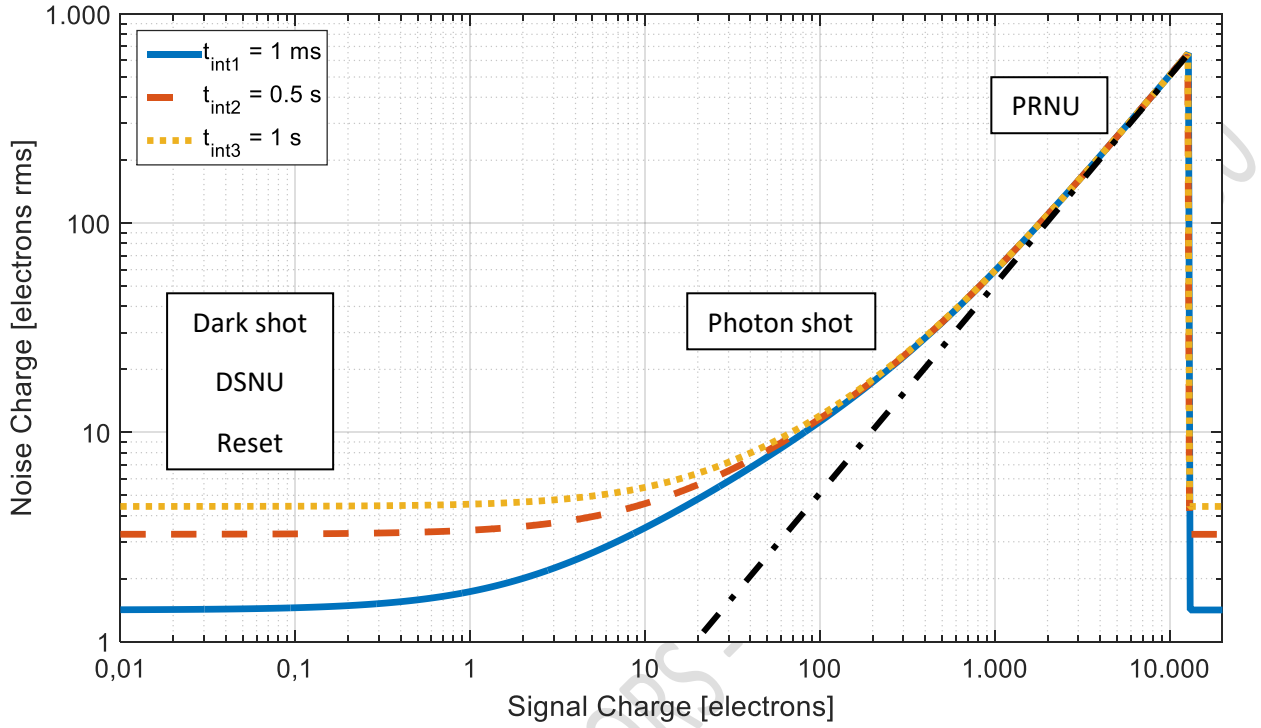

(i) Evaluate the sensor dynamic range.

(ii) Evaluate the sensor % PRNU and kTC noise.

The PTC is then captured at two further integration times, t_{int2} = 0.5 s and t_{int3} = 1 s (represented in the graph as a dashed and a dotted curve, respectively).

(iii) Evaluate the sensor dark current density and the % DSNU.

Physical Constants

q = 1.6 10-19 C
k_b = 1.38 10-23 J/K
T = 300 K (if not specified)
ε_0 = 8.85 10-12 F/m
ε_{rSi} = 11.7

(i)

The dynamic range is defined as the ratio between the maximum detectable signal and the minimum detectable one.

The full-well charge (FWC) can be easily inferred from the graph as the point on the x-axis where the considered curve drops to a meaningless value: 13000 electrons.

The minimum detectable signal can be found by choosing the point in the graph where noise on the y-axis equals the signal on the x-axis, i.e. where the signal-to-noise ratio is equal to 1. This point is found at 2 electrons for the solid curve.

The dynamic range can be thus directly evaluated as:

$$DR = 20\log_{10}\left(\frac{FWC}{\sigma}\right) = 20\log_{10}\left(\frac{13000\ e}{2\ e_{rms}}\right) = 76\ \text{dB}$$

(ii)

We know that spatial noise given by photo-response nonuniformity (PRNU) is proportional to the signal. By looking at the graph, here this happens, for the solid curve, in the signal range corresponding to 1'000-10'000 electrons.

By drawing the asymptotic line that fits the high signal level range of the PTC, one can infer the PRNU coefficient.

The asymptotic line crosses the 1 electron rms axis at an x-value of 20 electrons (see the graph). Hence,

$$\%PRNU = \frac{1}{N_{PRNU}} = \frac{1}{20} = 0.05 = 5\%$$

Among the signal-independent noise contributions, we know that there exist time-dependent (dark current shot noise and DSNU) and time-independent contributions (kTC noise and other read noise contributions). The latter become visible at short integration times.

Assuming that kTC noise is the dominant noise source at 1 ms integration time (we will later verify this hypothesis), its value can be directly inferred as the y-value of the PTC at very low signal levels:

$$\sigma_{kTC} = 1.4\ \text{electrons rms}$$

(iii)

As mentioned above, the y-value of the PTC at very low signal levels is dark noise (DN): dark noise is a combination of reset noise, that is independent from the integration time, dark current shot noise, that depends on the square root of the integration time, and dark-signal non-uniformity (DSNU), that depends linearly on the integration time.

Since from the dashed to the dotted curve the integration time is doubled, while extrapolated dark noise increases of a factor √2 only (from 3.1 to 4.4), we conclude that at these integration times our sensor is dark current shot noise limited, and the dark current can be estimated as

$$4.4 = \sigma_{dcsn} = \frac{\sqrt{q\ i_{dark}\ t_{int}}}{q} = \sqrt{\frac{i_{dark}}{q}t_{int}} = \sqrt{\frac{i_{dark}}{q}\ 1\ \text{s}} \quad \rightarrow \quad i_{dark} = 2.7\ \text{aA}$$

We observe that such a low dark current value is typical of 4T topologies where the pinning action of the surface P-type implant inhibits the collection of surface generated, perimeter dark-generated carriers.

Last Name __Girosco__ **Given Name** ___Pio__ **ID Number** ___20170130__

As the pixel is back-side illuminated, the fill factor can be assumed to be 100%, and thus the active area is assumed the same as the pixel area. The dark current density is thus

$$j_{dark} = \frac{i_{dark}}{l_{pix}^2} = 300\ \mathrm{nA/m^2} = 0.03\ \mathrm{nA/cm^2}$$

We do not have enough data to evaluate the DSNU, but given the observed square root dependency of noise with respect to signal, we can postulate that its contribution is negligible.

Finally, we observe that dark current shot noise at 1 ms integration time turns out to be 0.13 electrons rms, much lower than the previously-evaluated kTC noise (1.4 electrons rms). Hence, the assumption that kTC noise dominates with an integration time of 1 ms was valid.